Journal of Cerebral Blood Flow & Metabolism (2013) 33, 532–541

www.jcbfm.com

ORIGINAL ARTICLE

Kinetic analysis of the metabotropic glutamate subtype 5 tracer [^{18}F]FPEB in bolus and bolus-plus-constant-infusion studies in humans

Jenna M Sullivan[1,2], Keunpoong Lim[1], David Labaree[1], Shu-fei Lin[1], Timothy J McCarthy[3], John P Seibyl[4], Gilles Tamagnan[4], Yiyun Huang[1], Richard E Carson[1,2], Yu-Shin Ding[1,5] and Evan D Morris[1,2]

[^{18}F]FPEB is a positron emission tomography tracer which, in preclinical studies, has shown high specificity and selectivity toward the metabotropic glutamate receptor 5 (mGluR5). It possesses the potential to be used in human studies to evaluate mGluR5 function in a range of neuropsychiatric disorders, such as anxiety and Fragile X syndrome. To define optimal scan methodology, healthy human subjects were scanned for 6 hours following either a bolus injection ($n = 5$) or bolus-plus-constant-infusion ($n = 5$) of [^{18}F]FPEB. Arterial blood samples were collected and parent fraction measured by high-performance liquid chromatography (HPLC) to determine the metabolite-corrected plasma input function. Time activity curves were extracted from 13 regions and fitted by various models to estimate V_T and BP_{ND}. [^{18}F]FPEB was well fitted by the two-tissue compartment model, MA1 ($t^* = 30$), and MRTM (using cerebellum white matter as a reference). Highest V_T values were observed in the anterior cingulate and caudate, and lowest V_T values were observed in the cerebellum and pallidum. For kinetic modeling studies, V_T and BP_{ND} were estimated from bolus or bolus-plus-constant-infusion scans as short as 90 minutes. Bolus-plus-constant-infusion of [^{18}F]FPEB reduced intersubject variability in V_T and allowed equilibrium analysis to be completed with a 30-minute scan, acquired 90–120 minutes after the start of injection.

Journal of Cerebral Blood Flow & Metabolism (2013) **33,** 532–541; doi:10.1038/jcbfm.2012.195; published online 19 December 2012

Keywords: binding potential (BP_{ND}); bolus-plus-constant-infusion; glutamate; mGluR5; scan duration; total volume of distribution (V_T)

INTRODUCTION

Glutamate is the major excitatory neurotransmitter in the brain, and glutamatergic neurons account for ~90% of neurons in the human brain.[1] Glutamate receptors can be divided into two major types, ionotropic and metabotropic receptors. Metabotropic glutamate receptors can be further divided into three different groups and eight subtypes. The metabotropic glutamate receptor subtype 5 (mGluR5), a group I metabotropic glutamate receptor, is a G-protein-coupled receptor whose downstream action modulates a variety of pathways.[2] The mGluR5 has been implicated in a number of central nervous system disorders, including autism, Fragile X syndrome, Huntington's disease, addiction, anxiety, and depression.[3–9]

Three promising positron emission tomography (PET) ligands for mGluR5 have recently been synthesized: 3-(6-methyl-pyridin-2-ylethynyl)-cyclohex-2-enone-*O*-[^{11}C]methyl-oxime ([^{11}C]ABP688), 3-fluoro-5-(2-(2-[^{18}F](fluoromethyl)thiazol-4-yl)ethynyl)benzonitrile ([^{18}F]SP203), and 3-[^{18}F]Fluoro-5-[(pyridine-3-yl)ethynyl]benzonitrile ([^{18}F]FPEB). Both [^{11}C]ABP688 and [^{18}F]SP203 have been evaluated in humans. [^{11}C]ABP688 displayed high uptake in regions, such as the anterior cingulate and caudate, known to be rich in mGluR5.[10,11] The regional time activity curves (TACs) were well fitted by the two-tissue compartment (2TC) model and Logan graphical approach.[11] However, a [^{11}C]ABP688 test–retest study in humans showed a significant increase in binding parameters in the second scan, which is currently unexplained.[12] [^{18}F]SP203 also displayed regional uptake consistent with the known distribution of mGluR5. Its TACs were well fitted by the 2TC model,[13] and V_T values calculated by the equilibrium method were correlated with those from the 2TC model.[14] However, [^{18}F]SP203 has been shown to defluorinate in humans.[13]

[^{18}F]FPEB was the most successful among the three mGluR5 tracers characterized in rhesus monkeys by Hamill *et al.*[15] In preclinical studies, [^{18}F]FPEB displayed high specificity and affinity for mGluR5 as well as a regional uptake pattern consistent with the known distribution of mGluR5 in the brain.[16–18] Hence, [^{18}F]FPEB may have the potential to be used in humans to assess mGluR5 function in a variety of psychiatric and neurological disorders.

The goal of the present study was to determine the methodology and appropriate kinetic models for use of [^{18}F]FPEB in humans. We compared two different tracer administration paradigms, bolus and bolus-plus-constant infusion (B/I), to determine the optimum scanning protocol, and we evaluated

[1]Yale PET Center, Department of Diagnostic Radiology, Yale University, New Haven, Connecticut, USA; [2]Department of Biomedical Engineering, Yale University, New Haven, Connecticut, USA; [3]Pfizer Global R&D, Groton, Connecticut, USA and [4]Institute for Neurodegenerative Disorders, New Haven, Connecticut, USA. Correspondence: Dr ED Morris, Positron Emission Tomography (PET) Center, Yale University, 801 Howard Avenue, PO Box 208048, New Haven, CT 06520-8048, USA.
E-mail: evan.morris@yale.edu
This study was supported by the Yale Pfizer Bioimaging Alliance. This publication was also made possible by CTSA Grant Number UL1 RR024139 from the National Center for Research Resources (NCRR), a component of the National Institutes of Health (NIH), and NIH roadmap for Medical Research. Its contents are solely the responsibility of the authors and do not necessarily represent the official view of NCRR or NIH.
[5]Present address: Department of Radiology, NYU Langone Medical Center, 660 First Avenue, New York, NY 10016, USA.
Received 29 August 2012; revised 6 November 2012; accepted 23 November 2012; published online 19 December 2012

multiple quantification methods to estimate [^{18}F]FPEB total volume of distribution (V_T) and binding potential (BP_{ND}).

MATERIALS AND METHODS

Subjects

Nine healthy volunteers (5 M, 4 F) were recruited from the community through posted advertisements as approved by the Western Institutional Review Board (WIRB) and the Yale University Human Investigations Committee (HIC). All subjects underwent a complete physical examination before the study, including medical history, electrocardiogram, blood work, urinalysis, and urine toxicology screen. Subjects were screened via SCID (Structured Clinical Interview for DSM Disorders) for lifetime personal or family history of DSM IV axis I or axis II disorders. Only subjects without a history of neurological or psychiatric disorder were included in this study. Written informed consent was obtained from all subjects before the study after complete explanation of the study procedures.

Radiochemistry: Synthesis of 3-[^{18}F]Fluoro-5-(2-pyridinylethynyl)benzonitrile ([^{18}F]FPEB)

Aqueous [^{18}F]fluoride was produced via the $^{18}O(p,n)^{18}F$ reaction using a GE PETtrace cyclotron (General Electric Healthcare, Waukesha, WI, USA). The [^{18}F]F^- in [^{18}O]H_2O was loaded onto a Chromafix 30-PS-HCO3 cartridge and eluted into the graphite reactor of a GE FX_{F-N} chemistry module with a solution of 7.14 mg Kryptofix K_{222} and 0.743 mg K_2CO_3 in 1 mL CH_3CN/water (1:0.4 v/v). The solvent was evaporated at 70 °C at reduced pressure (~33 kPa) under an Ar stream for 5 minutes. A 1-mL aliquot of CH_3CN was added and evaporation resumed at 70 °C for 3 minutes, then another aliquot of CH_3CN (1 mL) was added and evaporation continued at 100 °C for another 5 minutes. The Ar flow was stopped and any remaining solvent was evaporated at 100 °C at reduced pressure (~8 kPa) for 5 minutes. After cooling to 60 °C, 1.0 mg of 3-nitro-5-[(pyridine-2-yl)ethynyl]benzonitrile ([^{18}F]FPEB precursor) in 1.5 mL of anhydrous dimethyl sulfoxide was added to the reactor. The reaction vessel was sealed, stirred, and heated at 150 °C for 15 minutes then cooled to 50 °C. Water (6.75 mL) was added to the reaction vessel and the mixture was loaded onto a C-18 SepPak Light cartridge. The crude product trapped on the SepPak Light cartridge was eluted with EtOH (1 mL) into a receiving vial containing H_2O (2.5 mL) and the mixture loaded onto a Luna C18(2) semipreparative high-performance liquid chromatography (HPLC) column (10×250 mm^2, 10 μm). The column was eluted with EtOH/H_2O (38:62 v/v) at a flow rate of 5 mL/min. The product peak fraction, collected at 28–31 minutes, was diluted with H_2O (15 mL) and loaded onto a second C18 SepPak Light cartridge, which was then washed with H_2O (15 mL) and dried. The final product was eluted from the SepPak Light with EtOH (1 mL) followed by USP saline (3 mL) into a product vial containing USP saline (7 mL). The resulting solution was passed through a 0.22 μm Millipore Millex GV filter into a sterile dose vial. Radiochemical purity and specific activity of the final product was determined by HPLC analysis with a Luna C18(2) column (4.6×250 mm^2, 5 μm) eluting with CH_3CN/aqueous 0.1% TFA (40:60, v/v) at a flow rate of 2 mL/min. The final product was >99% chemically pure and >98% radiochemically pure. Specific activity at end-of-synthesis was 207.2 ± 70.3 MBq/nmol ($n = 10$). Radiochemical yield was 2.2% ± 0.9% ($n = 10$), based on the amount of radioactivity remaining in the reaction vessel after drying and uncorrected for decay.

Positron Emission Tomography Imaging

Subjects (Table 1) were scanned for up to 6 hours on the High Resolution Research Tomograph (HRRT, Siemens/CTI, Knoxville, TN, USA) after either a bolus ($n = 5$) or B/I ($n = 5$) of [^{18}F]FPEB. Nine subjects were included in this study, but one subject was scanned under both tracer administration paradigms. This resulted in $n = 5$ subjects for both bolus and B/I scan groups. Scans were separated by 2 months in the subject who was scanned twice. Each 360-minute scan was divided into three sessions (0–120 minutes, 150–240 minutes, and 270–360 minutes) with 30 minute breaks between sessions during which time the subject was taken off the scanner bed to void. During B/I scans, subjects continued to be infused during the breaks. Transmission scans were conducted immediately before each dynamic scan session for attenuation correction.

Table 1. Subject demographics and tracer dose information

	Bolus	*B/I*
N	5	5
Gender	4 M, 1 F	2 M, 3 F
Age (years)	25 ± 5	23 ± 4
Weight (kg)	84.0 ± 16.0	71.5 ± 15.5
Dose (MBq)	173.9 ± 3.7	166.5 ± 22.2
SA @ TOI (MBq/nmol)	144.3 ± 44.4	181.3 ± 62.9
Injected mass (μg)	0.3 ± 0.1	0.4 ± 0.2

Total injected mass was limited to a maximum of 0.93 μg per injection. [^{18}F]FPEB dosimetry was evaluated in rhesus monkeys by Belanger *et al.*[19] and extrapolated to humans. Upon extrapolation to humans, Belanger *et al.*[19] found that the critical organ is the upper large intestine (0.20 mGy/MBq, i.e., 0.74 rad/mCi). From this, we estimated the maximum allowable injected dose of [^{18}F]FPEB to be 250 MBq per single injection. Each subject received no more than 185 MBq of [^{18}F]FPEB per injection (Table 1).

Special requirements were found for long infusions of [^{18}F]FPEB. Large bore glass (20 mL glass syringe, Tomopal, Sacramento, CA, USA; 1000 series 25 mL GasTight syringe, Hamilton, Reno, NV, USA) or plastic (30 mL BD Luer-Lok tip syringe, BD, Franklin Lakes, NJ, USA) syringes and PTFE tubing (PFTE-tube, 100 cm, Fluorplast Oy, Ab, PETALAX, Finland) were used to deliver [^{18}F]FPEB during B/I studies. Despite successful bolus experiments with plastic syringes and tubing, these materials were found to retain a substantial amount of [^{18}F]FPEB activity during the infusion period of B/I experiments. Retention was detected by measuring residual radioactivity in these materials at the end of the study, following a saline flush to remove any tracer solution remaining in the syringes or tubing. We prevented retention of radioactivity by further diluting the tracer solution with sterile saline in large bore plastic syringes or by using glass syringes, and by using PTFE tubing for tracer delivery.

An optical tracking system (Vicra, NDI Systems, Waterloo, Canada) was used to measure and record subject head movement during each scan. A rigid tool with reflective spheres was attached to each subject's head via a swim cap, and subject motion was recorded at a rate of 20 Hz. Listmode dynamic scan data were collected and reconstructed (reconstructed image resolution ~3 mm) with all corrections (randoms, scatter, dead time, attenuation, normalization, and motion) by the MOLAR algorithm.[20] In addition to the event-by-event motion correction performed during the reconstruction, software motion correction was also performed by registering each frame to an early summed image (0 to 10 minutes) using FLIRT (FSL 3.2, Analysis Group, FMRIB, Oxford, UK).

Before PET imaging, each subject received a structural MRI (magnetic resonance imaging) on a 3T whole-body Trio scanner (Siemens Medical Systems, Erlanger, Germany) using a 3D MPRAGE MR pulse sequence with TE = 3.3 milliseconds and flip angle = 7 degrees. Slice thickness was 1.0 mm and pixel size was 0.98×0.98 mm^2. For each subject, PET images were registered to the structural MRI for image analysis.

Input function

Input functions corresponding to the arterial blood concentration corrected for the presence of radioactive metabolites were generated for all scans. Arterial blood was counted for radioactivity by an automated system (PBS-101, Veenstra Instruments, Joure, The Netherlands) for the first 7 minutes of each study. Individual arterial and venous blood samples were also manually drawn at discrete time points and counted during each study. The plasma TAC for the first 7 minutes of each study was estimated from the whole blood TAC measured by the automated system. The ratio of the whole blood to plasma concentration was calculated for each sample collected from 3 to 30 minutes. The whole-blood-to-plasma ratio was fit to a linear function and extrapolated for 0–7 minutes. The early and late parts of the plasma curve were merged and the complete plasma curve was smoothed by fitting with a bounded sum of one to three exponentials.

An ultrafiltration-based method was used for measuring the unbound portion (free fraction, f_p) of [^{18}F]FPEB in plasma. In a volume no greater than 0.1 mL, 1.85 MBq of [^{18}F]FPEB was spiked in a 6.0-mL arterial blood sample that was taken immediately before tracer injection. After 10 minutes incubation at room temperature, the spiked blood sample was centrifuged for 5 minutes at 2,930 g. Spiked plasma (0.3 mL) was loaded onto the reservoir of a Millipore Centrifree (Billerica, MA, USA) micropartition device in triplicate and centrifuged at 1,228 g for 20 minutes. The f_p was determined by calculating the ratio of the radioactivity concentration of the unbound [^{18}F]FPEB passed through the filter to the total activity in plasma.

Analysis of radiotracer metabolism in the plasma was performed from arterial blood samples collected at 3, 8, 15, 30, 60, 90, 120, 180, and 240 minutes after injection and also from venous blood samples drawn at 60, 90, 120, 180, and 240 minutes after injection. Plasma metabolite analysis was performed using the column switching HPLC method[21] to determine the parent fraction. In short, plasma samples were treated with urea (8 M) and citric acid (50 mM) and loaded onto the capture column ($19 \times 4.6\,mm^2$, self-packed with Phenomenex SPE C18 Strata-X sorbent), eluting with 1% acetonitrile in water at a flow rate of 2 mL/min. After 4 minutes, the trapped activity on the capture column was back-flushed onto an analytical column (Phenomenex Luna, Torrance, CA, USA, C18(2), $4.6 \times 250\,mm^2$, 5 μm), eluting with 60% acetonitrile in 50 mM ammonium acetate, pH 6.8 at a flow rate of 1.25 mL/min. The HPLC eluent was fraction-collected with an automated collector (Model CF-1, Spectrum Chromatography, Houston, TX, USA) and the fraction counted with an automatic gamma well-counter (Wizard,[2] Perkin-Elmer, Waltham, MA, USA). The unmetabolized parent fraction was determined as the ratio of the sum of radioactivity in fractions containing the parent compound to the total amount of radioactivity collected, and fitted with a bounded sum of two exponentials. The final plasma input function was calculated as the product of the total plasma curve and the parent fraction curve.

Measurement of regional time activity curves

To compute regional TACs, a summed PET image (0–10 minutes) was registered to each subject's T1-weighted MR image using a six-parameter mutual information algorithm (FLIRT, FSL 3.2, Analysis Group, FMRIB, Oxford, UK), which was then registered to an MR template by a 12-parameter affine transformation. Regions of interest (ROIs) from the AAL (Anatomical Automatic Labeling for SPM2) template were defined on the MR template. Time activity curves were extracted from the caudate ($16\,cm^3$), cerebellum gray matter ($84\,cm^3$), cerebellum white matter ($6\,cm^3$), anterior cingulate ($22\,cm^3$), posterior cingulate ($6\,cm^3$), frontal cortex ($256\,cm^3$), hippocampus ($15\,cm^3$), occipital cortex ($81\,cm^3$), pallidum ($5\,cm^3$), putamen ($17\,cm^3$), temporal cortex ($172\,cm^3$), and thalamus ($17\,cm^3$). Note: the cerebellum white matter ROI was drawn, according to the AAL template, on the MR template deep within the cerebellum. No white matter/gray matter segmentation was applied.

Infusion paradigm

To determine the tracer infusion schedule for B/I experiments, the K_{bol} (the magnitude of the bolus component in minutes)[22] for [18]FPEB in humans was estimated from TACs from bolus studies. The K_{bol} that was selected for use in the B/I experiments was that for which both high and low specific binding regions (e.g., anterior cingulate and cerebellum gray matter) were predicted to reach equilibrium quickly. Individual K_{bol} values were estimated from the five bolus subjects, the average of which was found to be 190 ± 12 minutes. Thus for B/I studies, the K_{bol} value of 190 minutes was used.

Kinetic analysis

Regional TACs were fitted by three different models to estimate total volume of distribution (V_T) of [18]FPEB: 1TC and 2TC models and the multilinear analysis, MA1.[23] Binding potential (BP_{ND}) was calculated from 2TC V_T values and estimated by reference tissue models (SRTM and SRTM2)[24,25] and multilinear graphical analysis (MRTM and MRTM2)[26] using the cerebellum white matter as a reference region (see Discussion). Parametric images of V_T and BP_{ND} were generated with MA1 and MRTM2.

For all model fitting, parameters were estimated using weighted least squares, with weights based on noise-equivalent counts from each frame. Nonlinear parameter estimation was performed using a Marquardt-Levenberg algorithm.[27] The t^* value for multilinear graphical analyses (MA1, MRTM, and MRTM2) was selected based on visual inspection of MA1 fits. For reference tissue methods, TACs from the cerebellum white matter were presmoothed by fitting to a sum of exponentials. In SRTM2 and MRTM2 analyses, k_2' was fixed to the median k_2' value estimated from all voxels during a first-pass of each analysis.

In addition to dynamic modeling analysis, in B/I studies, V_T and BP_{ND} were estimated by equilibrium analysis (EQ)[28,29] using 90–120 minutes of data postinjection. We considered [18]FPEB to be in equilibrium in the tissue and plasma when average V_T change across all regions and plasma was less than or equal to $\pm 10\%$ per hour. Percent change in V_T per hour ($\%\Delta V_T/hour|_{90-120}$) was calculated as the slope of a line fit to these data (90–120 minutes postinjection), divided by the mean V_T value (multiplied by 60 to convert from minutes to hours). V_T was calculated as the ratio of tissue concentration to metabolite-corrected arterial plasma concentration at equilibrium. BP_{ND} was estimated as the target tissue concentration minus the reference relative to the reference tissue concentration. EQ was also used to generate parametric images of V_T and BP_{ND}.

Effect of scan duration

Dynamic scan data of decreasing duration were analyzed to determine the effect of scan duration on V_T. V_T was estimated by 2TC for each scan while fit duration was decreased from 360 to 30 minutes in steps of 30 minutes.

RESULTS

Input Function

[18]FPEB plasma free fraction, f_p, was $4.7\% \pm 0.6\%$ in bolus studies ($n = 5$) and $4.6\% \pm 0.5\%$ in B/I studies ($n = 5$). [18]FPEB was quickly metabolized; unchanged [18]FPEB represented $19\% \pm 3\%$ ($n = 5$) of total arterial plasma radioactivity at 30 minutes, $13\% \pm 1\%$ at 90 minutes ($n = 5$), $9\% \pm 1\%$ at 240 minutes ($n = 4$), and $7\% \pm 1\%$ at 360 minutes ($n = 3$) in bolus studies. In venous plasma, [18]FPEB represented $15\% \pm 1\%$ ($n = 4$) and $11\% \pm 0.3\%$ ($n = 3$) of total plasma activity in bolus studies at 90 and 240 minutes, respectively. Arterial parent fraction of [18]FPEB was higher in B/I studies than bolus studies at all time points. [18]FPEB represented $29\% \pm 3\%$ ($n = 5$) of total B/I arterial plasma radioactivity at 30 minutes, $25\% \pm 3\%$ at 90 minutes ($n = 5$), $20\% \pm 3\%$ at 240 minutes ($n = 5$), and $17\% \pm 2\%$ at 360 minutes ($n = 4$). [18]FPEB represented $23\% \pm 3\%$ ($n = 4$) and $19\% \pm 2\%$ ($n = 5$) of total B/I venous plasma activity at 90 and 240 minutes, respectively.

In B/I studies, mean (90–240 minutes) metabolite-corrected arterial plasma concentration was $12\% \pm 6\%$ ($n = 5$) higher ($P = 0.09$, two-tailed unpaired t-test) than metabolite-corrected venous plasma concentration. Total arterial plasma concentration was $7\% \pm 5\%$ ($n = 5$) higher ($P = 0.20$, two-tailed unpaired t-test) than total venous plasma concentration. Mean (90–240 minutes) arterial parent fraction was $7\% \pm 3\%$ ($n = 5$) higher ($P = 0.39$, two-tailed unpaired t-test) than venous parent fraction.

One subject from each tracer administration paradigm, bolus and B/I, was unable to complete the full 360-minute scan; a subject from the bolus group was only able to complete 120 minutes of scanning, and a separate subject from the B/I group was only able to complete 250 minutes of scanning. Additionally, metabolite analyses were unavailable for venous plasma from one bolus subject, venous plasma at the 90-minute time point for one B/I subject, and arterial plasma at the 360-minute time point for one bolus subject. As such, parent fractions are reported above for the number of subjects and time points at which they are available.

Time activity curves

Figure 1 shows TACs with model fits from selected regions. The highest concentrations of [18]FPEB were in the putamen and anterior cingulate, and the lowest concentrations were in the thalamus, cerebellum gray matter, and cerebellum white matter. Breaks between scanning sessions are visible as breaks in TACs. Good continuity appears in the curves despite these breaks.

Total distribution volume (V_T) estimation

The highest V_T values were observed in the anterior cingulate, putamen, temporal cortex, and caudate. V_T values were lowest in the thalamus, posterior cingulate, pallidum, and cerebellum (Table 2). The 2TC model provided better fits than the 1TC model to both bolus and B/I data (Figure 1A). The residual sum of squares and Akaike information criterion were lower for 2TC fits than 1TC fits in all subjects and regions. F-tests indicated that 2TC provided significantly ($P < 0.05$) better fits than the 1TC in all subjects and regions. Despite being the poorer model for [18]FPEB data, V_T estimates from 1TC agreed extremely well with those from 2TC in all regions in both bolus and B/I studies: $V_T^{1TC} = 1.01 \times V_T^{2TC} - 0.60$,

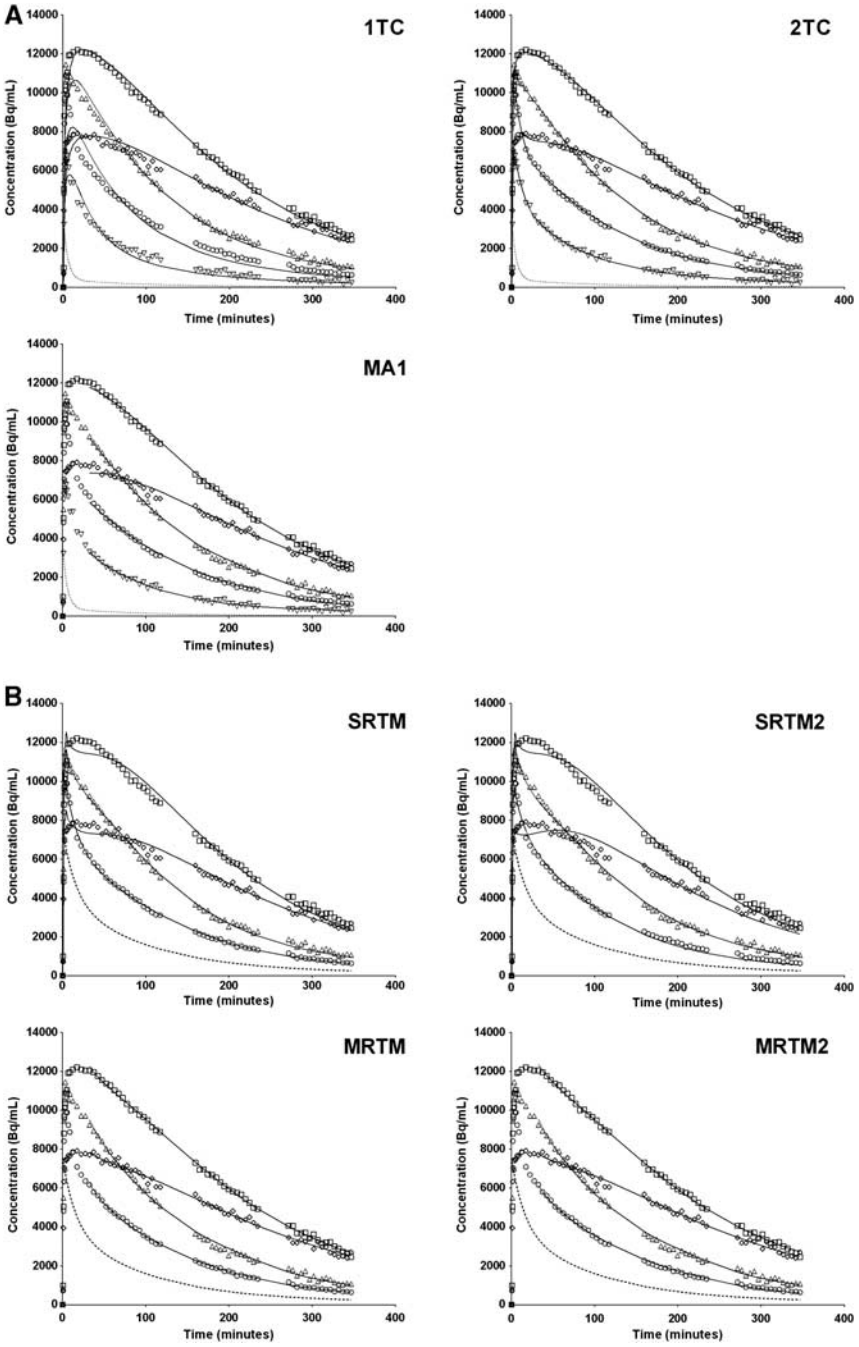

Figure 1. Representative bolus time activity curves and fits from selected regions: anterior cingulate (□), thalamus (Δ), hippocampus (◇), cerebellum gray matter (○), and cerebellum white matter (▽). (**A**) One-tissue compartment model (1TC), two-tissue compartment model (2TC), and MA1 ($t^* = 30$) fits are shown as solid lines. Dotted line is the fitted metabolite-corrected arterial input. (**B**) SRTM, SRTM2, MRTM ($t^* = 30$), and MRTM2 ($t^* = 30$) fits are shown as solid lines. Dashed line is the cerebellum white matter input (sum of exponentials fit to cerebellum white matter data).

$R^2 = 0.9993$, $n = 104$, 8 scans × 13 ROIs (note: results are reported from subjects who were able to complete the full 360 minutes of scanning). MA1 ($t^* = 30$) provided good fits to both bolus and B/I data (Figure 1A), and V_T values estimated by MA1 were in virtually perfect agreement with estimates from 2TC: $V_T^{MA1} = V_T^{2TC} + 0.03$, $R^2 = 0.9999$, $n = 104$. Parametric images of V_T estimated by MA1 from a bolus study are shown in Figure 2C.

Mean V_T values estimated by 2TC from B/I studies ($n = 4$) were lower than those from bolus studies ($n = 4$) in all regions except the cerebellum gray matter, cerebellum white matter, hippocampus, and thalamus (Figure 3A; Table 2). Intersubject variability in V_T estimated by 2TC was lower for B/I studies than bolus studies in all regions (11% ± 3% versus 20% ± 3% mean intersubject COV across all regions).

K_1 value estimation in bolus studies

K_1 values (estimated from bolus studies by 2TC) varied by region. Highest estimated K_1 values were in the putamen (0.51 ± 0.04 mL/min/cm^3, $n = 4$), thalamus (0.50 ± 0.03, $n = 4$), and frontal cortex (0.47 ± 0.05, $n = 4$). Lowest estimated K_1 values were in the cerebellum white matter (0.30 ± 0.04, $n = 4$), hippocampus

Table 2. Regional total volume of distribution (V_T) and binding potential (BP_{ND}) estimated from bolus and bolus-plus-constant-infusion studies of [^{18}F]FPEB in healthy human subjects

Region	*Total volume of distribution, V_T (mL/cm^3)*							*Binding potential, BP_{ND} (unitless)*								
	Bolus			*Bolus-plus-constant-infusion*				*Bolus*					*Bolus-plus-constant-infusion*			
	1TC	*2TC*	*MA1*	*1TC*	*2TC*	*MA1*	*EQ*	*2TC*	*SRTM*	*SRTM2*	*MRTM*	*MRTM2*	*2TC*	*MRTM*	*MRTM2*	*EQ*
Caudate	25.1 ± 4.8 (19%)	25.3 ± 4.8 (19%)	25.3 ± 4.9 (19%)	24.2 ± 2.1 (9%)	24.7 ± 1.9 (8%)	24.7 ± 2.0 (8%)	25.9 ± 2.2 (9%)	3.8 ± 0.4 (11%)	3.7 ± 0.4 (12%)	3.7 ± 0.4 (12%)	3.8 ± 0.5 (12%)	3.8 ± 0.5 (13%)	3.6 ± 0.5 (14%)	3.5 ± 0.6 (16%)	3.5 ± 0.6 (16%)	3.3 ± 0.3 (10%)
Cerebellum gray matter	8.7 ± 2.3 (26%)	9.4 ± 2.3 (25%)	9.5 ± 2.3 (25%)	9.3 ± 0.9 (10%)	10.0 ± 0.9 (9%)	10.0 ± 0.9 (9%)	11.4 ± 1.1 (10%)	0.8 ± 0.2 (31%)	0.8 ± 0.2 (31%)	0.7 ± 0.2 (31%)	0.8 ± 0.3 (35%)	0.8 ± 0.2 (31%)	0.9 ± 0.2 (20%)	0.8 ± 0.2 (20%)	0.8 ± 0.2 (21%)	0.9 ± 0.2 (18%)
Cerebellum white matter	4.8 ± 0.9 (20%)	5.2 ± 0.9 (18%)	5.3 ± 0.9 (18%)	4.9 ± 0.7 (14%)	5.4 ± 0.8 (15%)	5.4 ± 0.8 (14%)	6.1 ± 1.0 (16%)	—	—	—	—	—	—	—	—	—
Anterior cingulate	29.7 ± 5.3 (18%)	30.0 ± 5.3 (18%)	30.0 ± 5.2 (17%)	28.4 ± 3.8 (13%)	29.0 ± 3.7 (13%)	29.0 ± 3.8 (13%)	30.0 ± 4.5 (15%)	4.8 ± 0.5 (10%)	4.6 ± 0.4 (9%)	4.5 ± 0.4 (9%)	4.7 ± 0.4 (9%)	4.7 ± 0.4 (9%)	4.4 ± 0.4 (8%)	4.3 ± 0.4 (10%)	4.3 ± 0.4 (10%)	3.9 ± 0.5 (12%)
Posterior cingulate	14.4 ± 3.6 (25%)	14.8 ± 3.6 (24%)	14.9 ± 3.6 (24%)	12.8 ± 0.9 (7%)	13.3 ± 1.1 (8%)	13.3 ± 1.1 (8%)	15.1 ± 1.2 (8%)	1.8 ± 0.5 (29%)	1.8 ± 0.5 (30%)	1.8 ± 0.5 (31%)	1.8 ± 0.5 (28%)	1.8 ± 0.5 (29%)	1.5 ± 0.3 (19%)	1.5 ± 0.3 (21%)	1.5 ± 0.3 (21%)	1.5 ± 0.3 (19%)
Frontal	24.2 ± 6.0 (25%)	24.5 ± 6.0 (24%)	24.5 ± 6.0 (24%)	22.7 ± 1.9 (8%)	23.3 ± 1.8 (8%)	23.4 ± 1.9 (8%)	25.2 ± 1.8 (7%)	3.6 ± 0.5 (14%)	3.5 ± 0.5 (15%)	3.5 ± 0.5 (15%)	3.6 ± 0.5 (14%)	3.6 ± 0.5 (15%)	3.3 ± 0.5 (15%)	3.3 ± 0.5 (16%)	3.3 ± 0.5 (16%)	3.2 ± 0.4 (13%)
Hippocampus	22.8 ± 4.1 (18%)	23.2 ± 4.1 (18%)	23.2 ± 4.1 (18%)	22.5 ± 3.7 (16%)	23.4 ± 3.6 (16%)	23.4 ± 3.8 (16%)	22.1 ± 4.2 (19%)	3.5 ± 0.4 (11%)	3.3 ± 0.3 (10%)	3.2 ± 0.3 (10%)	3.4 ± 0.3 (10%)	3.4 ± 0.3 (9%)	3.3 ± 0.2 (6%)	3.3 ± 0.1 (3%)	3.2 ± 0.1 (4%)	2.6 ± 0.3 (11%)
Occipital	22.6 ± 4.8 (21%)	22.9 ± 4.7 (21%)	22.9 ± 4.8 (21%)	22.0 ± 2.6 (12%)	22.5 ± 2.6 (11%)	22.6 ± 2.6 (11%)	25.2 ± 2.7 (11%)	3.4 ± 0.3 (9%)	3.2 ± 0.3 (10%)	3.2 ± 0.3 (10%)	3.3 ± 0.3 (10%)	3.3 ± 0.3 (10%)	3.2 ± 0.3 (10%)	3.1 ± 0.3 (11%)	3.1 ± 0.3 (11%)	3.1 ± 0.2 (7%)
Pallidum	14.7 ± 2.8 (19%)	15.1 ± 2.8 (18%)	15.1 ± 2.8 (19%)	13.9 ± 2.4 (17%)	14.6 ± 2.2 (15%)	14.6 ± 2.3 (16%)	16.1 ± 2.6 (16%)	1.9 ± 0.3 (14%)	1.8 ± 0.3 (14%)	1.8 ± 0.3 (15%)	1.9 ± 0.3 (15%)	1.9 ± 0.3 (15%)	1.7 ± 0.4 (25%)	1.7 ± 0.4 (26%)	1.7 ± 0.4 (26%)	1.7 ± 0.4 (27%)
Parietal	24.0 ± 5.6 (23%)	24.3 ± 5.6 (23%)	24.4 ± 5.7 (23%)	22.8 ± 2.5 (11%)	23.3 ± 2.5 (11%)	23.4 ± 2.5 (11%)	25.5 ± 2.5 (10%)	3.6 ± 0.5 (13%)	3.5 ± 0.5 (13%)	3.5 ± 0.5 (13%)	3.6 ± 0.5 (13%)	3.6 ± 0.5 (13%)	3.3 ± 0.5 (15%)	3.3 ± 0.5 (16%)	3.3 ± 0.5 (16%)	3.2 ± 0.4 (11%)
Putamen	26.3 ± 5.2 (20%)	26.6 ± 5.2 (19%)	26.6 ± 5.2 (20%)	24.9 ± 2.6 (11%)	25.5 ± 2.7 (11%)	25.5 ± 2.7 (11%)	27.6 ± 3.1 (11%)	4.1 ± 0.5 (12%)	3.9 ± 0.5 (12%)	3.9 ± 0.5 (12%)	4.0 ± 0.5 (12%)	4.0 ± 0.5 (12%)	3.7 ± 0.6 (17%)	3.7 ± 0.7 (19%)	3.7 ± 0.7 (18%)	3.6 ± 0.6 (16%)
Temporal	27.5 ± 5.5 (20%)	27.8 ± 5.5 (20%)	27.8 ± 5.5 (20%)	26.1 ± 2.5 (10%)	26.7 ± 2.5 (9%)	26.6 ± 2.5 (10%)	28.0 ± 2.7 (10%)	4.3 ± 0.4 (10%)	4.1 ± 0.4 (10%)	4.1 ± 0.4 (10%)	4.3 ± 0.4 (10%)	4.2 ± 0.4 (10%)	4.0 ± 0.4 (9%)	3.9 ± 0.4 (11%)	3.9 ± 0.4 (11%)	3.6 ± 0.4 (10%)
Thalamus	16.1 ± 3.1 (19%)	16.5 ± 3.0 (18%)	16.5 ± 3.0 (18%)	16.1 ± 1.4 (9%)	16.6 ± 1.4 (9%)	16.7 ± 1.5 (9%)	19.0 ± 2.4 (13%)	2.1 ± 0.2 (12%)	2.1 ± 0.2 (11%)	2.1 ± 0.2 (12%)	2.1 ± 0.2 (11%)	2.1 ± 0.2 (11%)	2.1 ± 0.2 (11%)	2.1 ± 0.2 (11%)	2.1 ± 0.2 (11%)	2.1 ± 0.3 (14%)

Value are presented as mean ± s.d. COV is shown in parentheses. $n = 4$ for both bolus and B/I studies (one subject from each administration paradigm was unable to complete the full 360-minute scan).

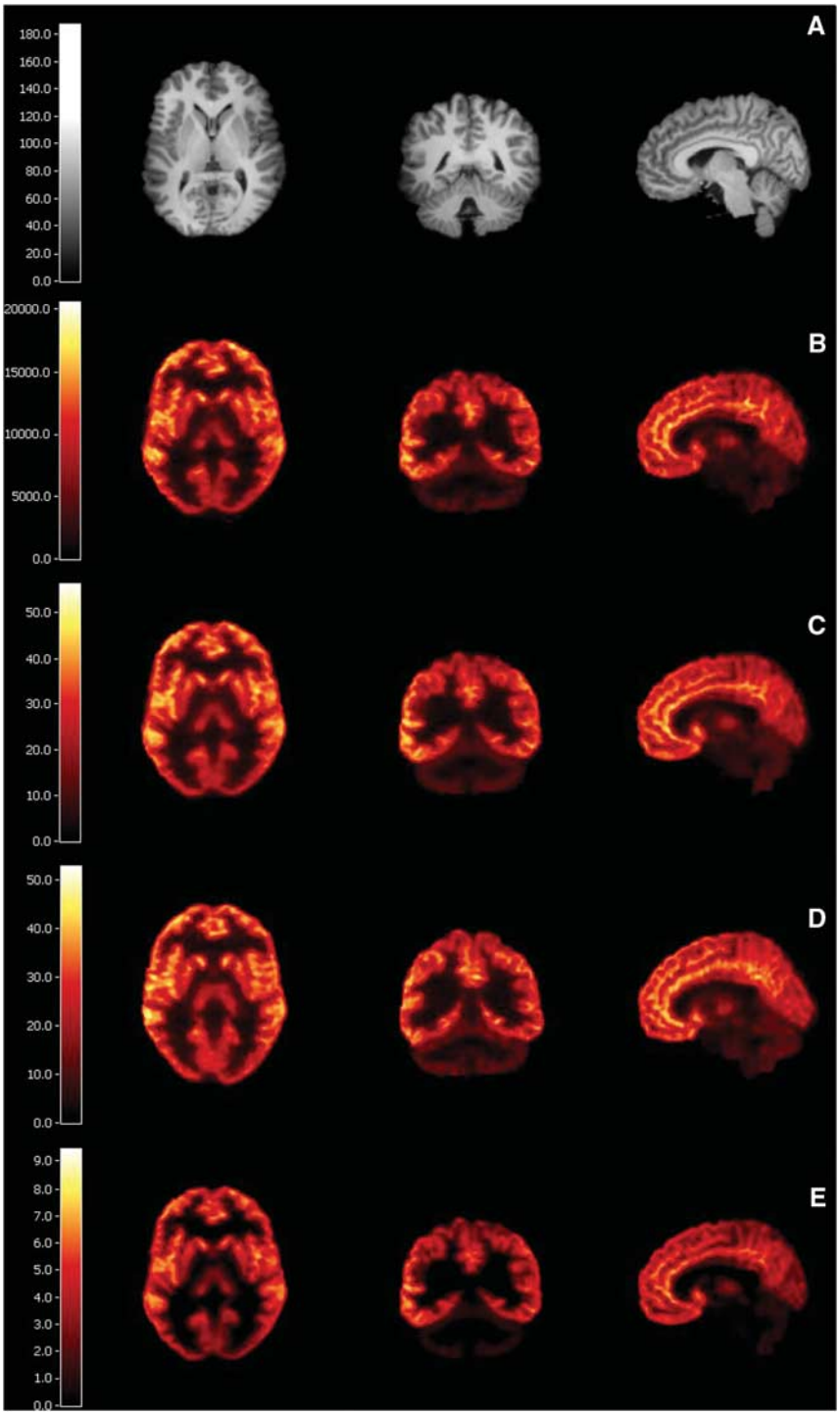

Figure 2. (**A**) Anatomic magnetic resonance image (MRI). (**B**) Summed image (90–120 minutes) from bolus study; units are Bq/mL. (**C**) Parametric total volume of distribution (V_T) image from bolus study estimated by MA1 ($t^* = 30$). (**D**) Parametric V_T from bolus-plus-constant-infusion (B/I) study calculated by the equilibrium method (90–120 minutes). (**E**) Parametric binding potential (BP_{ND}) image from bolus study estimated by MRTM2 ($t^* = 30$). Three views are shown for all images: transaxial, coronal, and sagittal.

(0.31 ± 0.01, $n = 4$), and pallidum (0.35 ± 0.02, $n = 4$). In all regions ($n = 52$), K_1 was $36\% \pm 11\%$ lower when estimated by 1TC than when estimated by 2TC.

Binding potential (BP_{ND}) estimation

Mean BP_{ND} values estimated by 2TC using the cerebellum white matter as reference ranged from a high of 4.8 ± 0.5 in the anterior cingulate to a low of 0.8 ± 0.2 in the cerebellum gray matter (Table 2). MRTM and MRTM2 ($t^* = 30$) provided visually better fits to bolus data than SRTM or SRTM2 (Figure 1B). In bolus studies, SRTM and SRTM2 underestimated BP_{ND} by $3.4\% \pm 1.2\%$ and $4.2\% \pm 1.7\%$, respectively, as compared with 2TC: $BP_{ND}^{SRTM} = 0.96 \times BP_{ND}^{2TC} + 0.02$, $R^2 = 0.9992$, $n = 48$; $BP_{ND}^{SRTM2} = 0.96 \times BP_{ND}^{2TC} - 0.01$, $R^2 = 0.9982$, $n = 48$. BP_{ND} values estimated by SRTM were significantly ($P < 0.05$, two-tailed paired *t*-test) lower than those

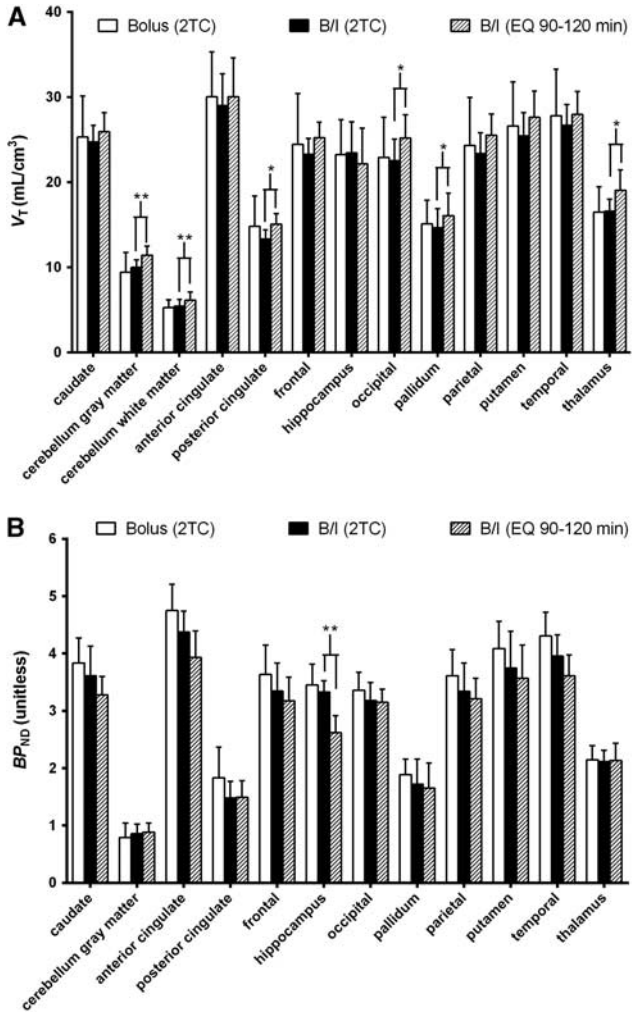

Figure 3. Comparison of regional (**A**) total volume of distribution (V_T) values and (**B**) binding potential (BP_{ND}) from bolus ($n=4$) and bolus-plus-constant-infusion (B/I, $n=4$) studies. Values are means and error bars are standard deviation. Parameter values shown are those estimated by the two-tissue compartment model (2TC) in both bolus and B/I studies and calculated by the equilibrium method (EQ) in B/I studies. $^{**}P<0.01$; $^{*}P<0.05$; paired two-tailed *t*-tests.

estimated by 2TC in all regions except the cerebellum gray matter. BP_{ND} values estimated by SRTM2 were significantly ($P<0.05$, two-tailed paired *t*-test) lower than those estimated by 2TC in all regions. BP_{ND} estimated by MRTM and MRTM2 provided better agreement with BP_{ND} estimated by 2TC: $BP_{ND}^{MRTM}=0.99\times BP_{ND}^{2TC}+0.01$, $R^2=0.9989$, $n=48$; $BP_{ND}^{MRTM2}=0.99\times BP_{ND}^{2TC}+0.01$, $R^2=0.9986$; $n=48$. BP_{ND} values estimated by MRTM were not significantly different than those estimated by 2TC in any region except the caudate and putamen. In the caudate and putamen, BP_{ND} values estimated by MRTM were significantly ($P<0.05$, two-tailed paired *t*-test) lower than those estimated by 2TC. BP_{ND} values estimated by MRTM2 were not significantly different than those estimated by 2TC in any region. Bolus study BP_{ND} parametric images from MRTM2 are shown in Figure 2E.

Since the statistical quality of the MRTM/MRTM2 images was good, parametric images with SRTM/SRTM2 were not produced given their poorer fits (Figure 1B) and slightly larger bias. SRTM and SRTM2 were not applied to B/I data for these same reasons. Like with bolus data, BP_{ND} estimated by MRTM and MRTM2 for B/I data was in excellent agreement with that estimated by 2TC: $BP_{ND}^{MRTM}=0.99\times BP_{ND}^{2TC}-0.01$, $R^2=0.9974$, $n=48$; $BP_{ND}^{MRTM2}=0.98\times BP_{ND}^{2TC}-0.01$, $R^2=0.9981$, $n=48$. BP_{ND} values estimated by MRTM in B/I studies were significantly ($P<0.05$, two-tailed paired *t*-test) lower than those estimated by 2TC in the frontal, occipital, parietal, and temporal cortices, and in the thalamus. BP_{ND} values estimated by MRTM2 in B/I studies were significantly ($P<0.05$, two-tailed paired *t*-test) lower than those estimated by 2TC in the caudate, posterior cingulate, frontal, occipital, parietal, and temporal cortices, and in the thalamus.

Mean BP_{ND} values (estimated by 2TC) were lower in B/I studies ($n=4$) than bolus studies ($n=4$) for all regions except the cerebellum gray matter and thalamus (Figure 3B; Table 2). Mean intersubject variability of BP_{ND} (estimated by 2TC) across all regions was $14\%\pm6\%$ for B/I studies and $15\%\pm8\%$ for bolus studies. There were no apparent differences in intersubject variation in BP_{ND} between analysis methods for a given injection approach.

Equilibrium method

Tissue TACs and arterial plasma curves appeared to flatten beginning at 90 minutes postinjection. Representative B/I TACs are shown in Figure 4. Average $\%\Delta V_T/\text{hour}|_{90-120}$ was $+2\%\pm8\%$ ($n=65$) for all regions and subjects from B/I studies. The cerebellum white matter and the hippocampus showed the largest $\%\Delta V_T/\text{hour}|_{90-120}$, $-10\%\pm10\%$ and $+10\%\pm5\%$ ($n=5$), respectively. $\%\Delta V_T/\text{hour}|_{90-120}$ was most variable across subjects in the cerebellum white matter, posterior cingulate ($+6\%\pm10\%$), and pallidum ($-2\%\pm11\%$).

EQ, applied to 90–120 minutes of data, overestimated V_T by $9\%\pm8\%$ compared with 2TC: $V_T^{EQ}=V_T^{2TC}+1.44$, $R^2=0.9555$, $n=52$ (Figure 3A). Significant V_T overestimation was seen in the cerebellum gray matter, cerebellum white matter, posterior cingulate, occipital cortex, pallidum, and thalamus (Figure 3A). Conversely, EQ underestimated BP_{ND} by $5\%\pm9\%$ compared with 2TC ($BP_{ND}^{EQ}=0.85\times BP_{ND}^{2TC}+0.25$, $R^2=0.9299$, $n=48$). Significant BP_{ND} underestimation was seen in only in the hippocampus (Figure 3B). Intersubject variability in V_T and BP_{ND} was similar for EQ and 2TC (Table 2). Parametric images of V_T estimated by EQ (90–120 minutes) are shown in Figure 2D.

Scan duration

In both bolus and B/I studies, scan duration could be decreased to 90 minutes without V_T bias or increased variability (Figure 5). V_T variability increased with scan durations below 90 minutes, and V_T values became negatively biased.

DISCUSSION

In healthy controls, we evaluated bolus and B/I administration paradigms of [18]FPEB and a variety of quantification techniques to determine the optimum methods to estimate V_T and BP_{ND} for [18]FPEB in humans.

The 2TC model provided better fits in all regions than the 1TC model. MA1 ($t^*=30$) fitted the data well and estimated V_T values nearly identical to those estimated by 2TC. MA1 ($t^*=30$) also produced high-quality parametric images from bolus and B/I scan data (Figure 2). MRTM and MRTM2 ($t^*=30$) both provided equally reliable estimates of BP_{ND}. MRTM2 produced the least noisy parametric BP_{ND} images, as assessed by visual inspection. SRTM and SRTM2 did not adequately fit the data and slightly underestimated BP_{ND} compared with 2TC. It has been shown that violation of SRTM model assumptions, such as the assumption that ROIs and the reference region can be described by 1TC models, can produce biased parameter estimates and poor fits.[25,30] Violation of either of these assumptions, or both of them by [18]FPEB may explain the poor fits by SRTM and SRTM2. MRTM does not assume a specific compartmental model

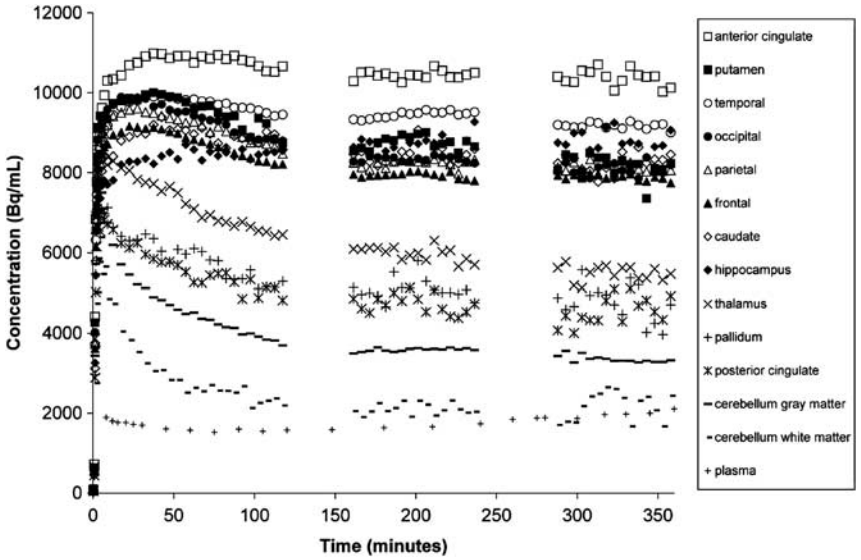

Figure 4. Representative time activity curves from a subject who received a bolus-plus-constant-infusion of [18F]FPEB.

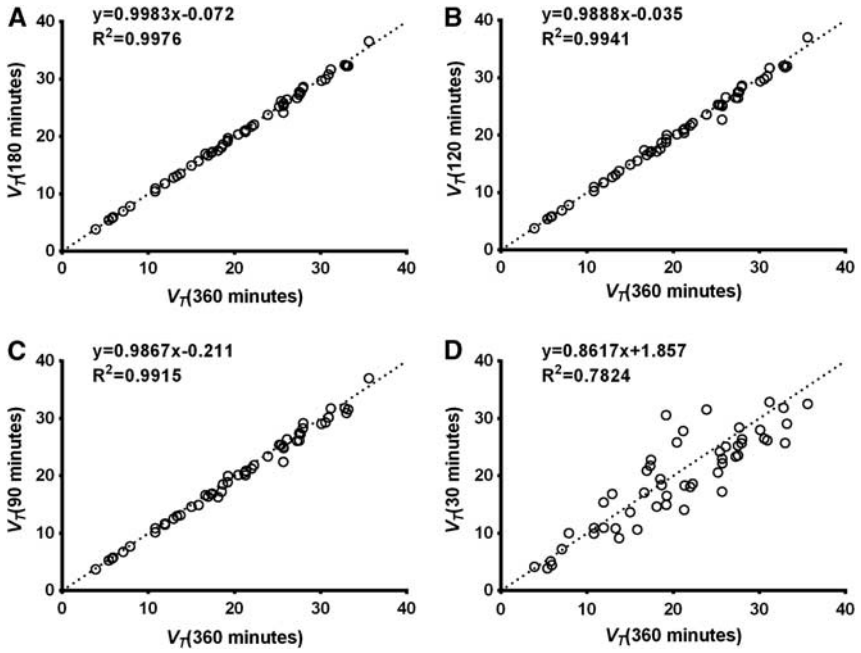

Figure 5. Effect of decreased scan duration on total volume of distribution (V_T) estimated by the two-tissue compartment model (2TC) in bolus studies. Correlation between V_T estimated from (**A**) 180, (**B**) 120, (**C**) 90, or (**D**) 30 minutes of data and 360 minutes of data ($n = 4$ subjects). Dotted line in each graph is line of identity. Correlation between V_T estimated from 60 minutes of data and 360 minutes of data is not shown but was similar to that for 90 minutes of data ($V_T^{60min} = 0.9824 \times V_T^{360min}$-0.4075, $R^2 = 0.9810$).

configuration and thus is less affected by violation of these assumptions.[26]

We calculated BP_{ND} using cerebellum white matter as the reference region. We selected this region to test BP_{ND} estimation methods because it showed the least specific binding by autoradiography[17] and had the lowest V_T (with reasonable intersubject variability). The cerebellum has been suggested as a reference region in preclinical studies with [11C]ABP688. Blocking studies conducted in rats with [11C]ABP688 found no displaceable binding in the cerebellum.[31] In the baboon, the cerebellum gray matter has been proposed as the reference region of choice, despite blocking studies which showed 20% specific binding of [11C]ABP688 in this region.[32] Given the known presence of mGluR5 in the cerebellum of humans,[17] it may not be an appropriate reference region. In addition, white matter regions may not have the same level of nondisplaceable binding (V_{ND}) as gray matter regions, thus use of cerebellar white matter may produce a biased estimate of BP_{ND}, even in the absence of specific binding. [18F]FPEB wash-in and wash-out the in cerebellum white matter appears to be similar to that of the cerebellum gray matter and other low-binding gray matter regions (Figure 1). This suggests no delay in delivery of or slower clearance of [18F]FPEB from the white matter, as has been reported with other tracers.[33–35] Ultimately, to confirm the absence (or presence) of a reference

region for [18F]FPEB blocking studies are needed. Until blocking studies are completed, the use of V_T as an outcome measure for [18F]FPEB may be most appropriate.

In our B/I scans with [18F]FPEB, equilibrium was achieved (according to the criteria of $\leqslant$10% average ΔV_T/hour$|_{90-120}$ across all regions) in all subjects. The largest ΔV_T/hour$|_{90-120}$ and largest variability in ΔV_T/hour$|_{90-120}$ were both observed in the cerebellum white matter ($-10\% \pm 10\%$). This, along with higher variability in other low-binding regions, may indicate that our selected K_{bol} (190 minutes) was biased towards high-binding regions. If lower-binding regions are of interest, a smaller K_{bol} may be preferred. Equilibrium (as assessed by ΔV_T/hour) did not improve at later scan times (120–360 minutes).

We investigated the B/I tracer administration paradigm because of its advantages over bolus injection.[36] B/I administration of tracer resulted in less intersubject variability in V_T estimated by 2TC (11% ± 3% versus 20% ± 3% in bolus studies), and a slight decrease in variability of BP_{ND} estimation (14% ± 6% versus 15% ± 8% in bolus studies) than bolus studies. Since B/I of tracer appears to provide no improvement in BP_{ND} intersubject variability, a bolus tracer administration paradigm may be sufficient if model-based estimates of BP_{ND} are to be used as the outcome measure (assuming that the cerebellum white matter is validated as an appropriate reference region). We doubt that the improvement in intersubject variability of V_T with B/I of tracer is a reflection of variance in specific binding, as if it were, we would expect to see the same improvement in variability with B/I of tracer in both V_T estimates and BP_{ND} estimates. It is more probable that the difference in variance of V_T reflects differences in variability of tracer uptake and washout between bolus and B/I groups.[36] Intersubject variability of K_1/k_2 was much in larger the bolus group than the B/I group (48% ± 12% versus 20% ± 12%). Another possibility is that the higher variability of V_T in bolus studies may be due to noise in the arterial input function (which is improved by B/I of tracer).

V_T values calculated by EQ were positively biased compared with 2TC, but intersubject variability in these measures was no worse than for 2TC. In low-binding regions (cerebellum, posterior cingulate, pallidum, and thalamus), V_T values calculated by EQ were significantly greater than those estimated by 2TC (Figure 3A). This difference may be caused, in part, by the greater ΔV_T/hour$|_{90-120}$ in these regions.

To successfully administer [18F]FPEB as a B/I, we had to overcome problems with retention of the tracer by conventional IV tubing and syringes. In early infusion studies using conventional 10 mL plastic syringes and IV tubing for tracer injection, we found that up to 75% of the tracer activity was retained by the tubing and the syringe over 3.5 hours (data not shown). We believe that the increased residence time of [18F]FPEB in the infusion promoted retention of [18F]FPEB by the syringe and IV tubing materials through a dipole interaction of [18F]FPEB molecules with bulk water in the saline delivery solution. Future [18F]FPEB studies should take this into account when deciding whether or not to administer the tracer as a B/I.

To examine whether or not venous blood could be used in lieu of arterial blood to estimate V_T at from EQ of B/I studies, we measured [18F]FPEB concentration and metabolites in both arterial and venous blood. Although we expected these values to be similar at equilibrium, both total plasma concentration and parent fraction were 7% lower in venous blood than arterial blood. This resulted in higher values when V_T was calculated by EQ (90–120 minutes) using metabolite-corrected venous plasma rather than metabolite-corrected arterial plasma data. Intersubject variability was also greater for V_T calculated by EQ (90–120 minutes) from venous plasma data (mean COV of 15% ± 3% versus 12% ± 4% for that calculated from arterial plasma). Given that total plasma concentrations and parent fractions were consistently lower in venous blood than arterial blood, this discrepancy may be due to procedural differences in analyzing arterial and venous samples, although to date, none have been identified. As the metabolite-corrected arterial-venous plasma difference has so far appeared to be consistent, it may be possible to use venous plasma in lieu of arterial plasma to estimate V_T in healthy controls. However, since this difference is not well understood, the decision to use venous plasma to estimate V_T at equilibrium should be considered carefully.

CONCLUSIONS

[18F]FPEB is an excellent tracer for the characterization of mGluR5 in humans. For kinetic modeling studies, bolus or B/I scans as short as 90 minutes are possible without increase in bias or noise. [18F]FPEB V_T can be reliably determined by 2TC, MA1 ($t^* = 30$), or the equilibrium approach. B/I of [18F]FPEB reduces intersubject variability and allows equilibrium analysis to be completed with a 30-minute static scan, acquired 90–120 minutes after start of injection; however, consideration must be given to the materials of the injection syringes and IV tubing to prevent tracer retention. [18F]FPEB BP_{ND} can be reliably estimated by MRTM, MRTM2, or the equilibrium approach, but until a reference region is fully validated, V_T should be estimated using an arterial input function.

DISCLOSURE/CONFLICT OF INTEREST

The authors declare no conflict of interest.

ACKNOWLEDGEMENTS

The authors thank the staff of the Yale University PET Center for their technical expertise and support.

REFERENCES

1 Shulman RG, Rothman DL (eds) *Brain Energetics and Neuronal Activity: Applications to fMRI and Medicine*. John Wiley & Sons, Ltd: Hoboken, NJ, 2004.
2 Ribeiro FM, Paquet M, Cregan SP, Ferguson SS. Group I metabotropic glutamate receptor signalling and its implication in neurological disease. *CNS Neurol Disord Drug Targets* 2010; **9**: 574–595.
3 Carroll FI. Antagonists at metabotropic glutamate receptor subtype 5: structure activity relationships and therapeutic potential for addiction. *Ann NY Acad Sci* 2008; **1141**: 221–232.
4 Olive MF. Metabotropic glutamate receptor ligands as potential therapeutics for addiction. *Curr Drug Abuse Rev* 2009; **2**: 83–98.
5 Osborne MP, Olive MF. A role for mGluR5 receptors in intravenous methamphetamine self-administration. *Ann N Y Acad Sci* 2008; **1139**: 206–211.
6 Bordi F, Ugolini A. Group I metabotropic glutamate receptors: implications for brain diseases. *Prog Neurobiol* 1999; **59**: 55–79.
7 Reissner KJ, Kalivas PW. Using glutamate homeostasis as a target for treating addictive disorders. *Behav Pharmacol* 2010; **21**: 514–522.
8 Guo Y, Wang HL, Xiang XH, Zhao Y. The role of glutamate and its receptors in mesocorticolimbic dopaminergic regions in opioid addiction. *Neurosci Biobehav Rev* 2009; **33**: 864–873.
9 Geisler S, Wise RA. Functional implications of glutamatergic projections to the ventral tegmental area. *Rev Neurosci* 2008; **19**: 227–244.
10 Ametamey SM, Treyer V, Streffer J, Wyss MT, Schmidt M, Blagoev M *et al.* Human PET studies of metabotropic glutamate receptor subtype 5 with 11C-ABP688. *J Nucl Med* 2007; **48**: 247–252.
11 Treyer V, Streffer J, Wyss MT, Bettio A, Ametamey SM, Fischer U *et al.* Evaluation of the metabotropic glutamate receptor subtype 5 using PET and 11C-ABP688: assessment of methods. *J Nucl Med* 2007; **48**: 1207–1215.
12 Delorenzo C, Kumar JS, Mann JJ, Parsey RV. *In vivo* variation in metabotropic glutamate receptor subtype 5 binding using positron emission tomography and [(11)C]ABP688. *J Cereb Blood Flow Metab* 2011 2169–2180.
13 Brown AK, Kimura Y, Zoghbi SS, Simeon FG, Liow JS, Kreisl WC *et al.* Metabotropic glutamate subtype 5 receptors are quantified in the human brain with a novel radioligand for PET. *J Nucl Med* 2008; **49**: 2042–2048.
14 Kimura Y, Simeon FG, Zoghbi SS, Zhang Y, Hatazawa J, Pike VW *et al.* Quantification of metabotropic glutamate subtype 5 receptors in the brain by an equilibrium method using 18F-SP203. *Neuroimage* 2012; **59**: 2124–2130.

15 Hamill TG, Krause S, Ryan C, Bonnefous C, Govek S, Seiders TJ *et al.* Synthesis, characterization, and first successful monkey imaging studies of metabotropic glutamate receptor subtype 5 (mGluR5) PET radiotracers. *Synapse* 2005; **56**: 205–216.
16 Wang JQ, Tueckmantel W, Zhu A, Pellegrino D, Brownell AL. Synthesis and preliminary biological evaluation of 3-[(18)F]fluoro-5-(2-pyridinylethynyl)benzonitrile as a PET radiotracer for imaging metabotropic glutamate receptor subtype 5. *Synapse* 2007; **61**: 951–961.
17 Patel S, Hamill TG, Connolly B, Jagoda E, Li W, Gibson RE. Species differences in mGluR5 binding sites in mammalian central nervous system determined using *in vitro* binding with [18F]F-PEB. *Nucl Med Biol* 2007; **34**: 1009–1017.
18 Patel S, Ndubizu O, Hamill T, Chaudhary A, Burns HD, Hargreaves R *et al.* Screening cascade and development of potential positron emission tomography radiotracers for mGluR5: *in vitro* and *in vivo* characterization. *Mol Imaging Biol* 2005; **7**: 314–323.
19 Belanger MJ, Krause SM, Ryan C, Sanabria-Bohorquez S, Li W, Hamill TG *et al.* Biodistribution and radiation dosimetry of [18 F]F-PEB in nonhuman primates. *Nucl Med Commun* 2008; **29**: 915–919.
20 Carson RE, Barker WC, Jeih-San L, Johnson CA. Design of a motion-compensation OSEM list-mode algorithm for resolution-recovery reconstruction for the HRRT. *Nuclear Science Symposium Conference Record 2003 IEEE* 2003, pp 3281–3285Vol.3285.
21 Hilton J, Yokoi F, Dannals RF, Ravert HT, Szabo Z, Wong DF. Column-switching HPLC for the analysis of plasma in PET imaging studies. *Nucl Med Biol* 2000; **27**: 627–630.
22 Carson RE, Channing MA, Blasberg RG, Dunn BB, Cohen RM, Rice KC *et al.* Comparison of bolus and infusion methods for receptor quantitation: application to [18F]cyclofoxy and positron emission tomography. *J Cereb Blood Flow Metab* 1993; **13**: 24–42.
23 Ichise M, Toyama H, Innis RB, Carson RE. Strategies to improve neuroreceptor parameter estimation by linear regression analysis. *J Cereb Blood Flow Metab* 2002; **22**: 1271–1281.
24 Lammertsma AA, Hume SP. Simplified reference tissue model for PET receptor studies. *Neuroimage* 1996; **4**: 153–158.
25 Wu Y, Carson RE. Noise reduction in the simplified reference tissue model for neuroreceptor functional imaging. *J Cereb Blood Flow Metab* 2002; **22**: 1440–1452.
26 Ichise M, Liow JS, Lu JQ, Takano A, Model K, Toyama H *et al.* Linearized reference tissue parametric imaging methods: application to [11C]DASB positron emission tomography studies of the serotonin transporter in human brain. *J Cereb Blood Flow Metab* 2003; **23**: 1096–1112.
27 Marquardt DW. An algorithm for least-squares estimation of nonlinear parameters. *J Soc Industrial Appl Math* 1963; **11**: 431–441.
28 Lassen NA. Neuroreceptor quantitation *in vivo* by the steady-state principle using constant infusion or bolus injection of radioactive tracers. *J Cereb Blood Flow Metab* 1992; **12**: 709–716.
29 Frey KA, Ehrenkaufer RL, Beaucage S, Agranoff BW. Quantitative *in vivo* receptor binding. I. Theory and application to the muscarinic cholinergic receptor. *J Neurosci* 1985; **5**: 421–428.
30 Slifstein M, Parsey RV, Laruelle M. Derivation of [(11)C]WAY-100635 binding parameters with reference tissue models: effect of violations of model assumptions. *Nucl Med Biol* 2000; **27**: 487–492.
31 Elmenhorst D, Minuzzi L, Aliaga A, Rowley J, Massarweh G, Diksic M *et al. In vivo* and *in vitro* validation of reference tissue models for the mGluR5 ligand [11C]ABP688. *J Cereb Blood Flow Metab* 2010; **30**: 1538–1549.
32 DeLorenzo C, Milak MS, Brennan KG, Kumar JS, Mann JJ, Parsey RV. *In vivo* positron emission tomography imaging with [11C]ABP688: binding variability and specificity for the metabotropic glutamate receptor subtype 5 in baboons. *Eur J Nucl Med Mol Imaging* 2011; **38**: 1083–1094.
33 Fodero-Tavoletti MT, Rowe CC, McLean CA, Leone L, Li QX, Masters CL *et al.* Characterization of PiB binding to white matter in Alzheimer disease and other dementias. *J Nucl Med* 2009; **50**: 198–204.
34 Ichise M, Golan H, Ballinger JR, Vines D, Blackman A, Moldofsky H. Regional differences in Technetium-99m-ECD clearance on brain SPECT in healthy subjects. *J Nucl Med* 1997; **38**: 1253–1260.
35 Wong K-P, Wardak M, Shao W, Dahlbom M, Kepe V, Liu J *et al.* Quantitative analysis of [18F]FDDNP PET using subcortical white matter as reference region. *Eur J Nucl Med Mol Imaging* 2010; **37**: 575–588.
36 Carson RE. PET physiological measurements using constant infusion. *Nucl Med Biol* 2000; **27**: 657–660.